J Solid State Electrochem (2012) 16:3667–3674
DOI 10.1007/s10008-012-1810-8

ORIGINAL PAPER

Surfactant-coassisted sol–gel synthesis to prepare $LiNi_yMn_yCo_{1-2y}O_2$ with improved electrochemical behavior

D. Bhuvaneswari · Gangulibabu · N. Kalaiselvi

Received: 23 May 2012 / Revised: 20 June 2012 / Accepted: 24 June 2012 / Published online: 8 July 2012

Abstract Layered $LiNi_yMn_yCo_{1-2y}O_2$ [y=0.5, 0.45, and 0.4] compounds with interconnected spherical particles are synthesized using a novel surfactant-coassisted sol–gel process. A combination of cetyltrimethyl ammonium bromide as surfactant and citric acid as chelating agent results in the formation of hydrophobically nucleated transparent gel, which upon furnace calcination yields phase pure and growth-controlled spherical particles of $LiNi_yMn_yCo_{1-2y}O_2$ [y=0.5, 0.45, and 0.4] compounds. The compounds containing Co^{3+} ions, viz., $LiNi_{0.45}Mn_{0.45}C_{0.1}O_2$ and $LiNi_{0.4}Mn_{0.4}Co_{0.2}O_2$ cathodes, exhibit good cation ordering and better electrochemical performance than $LiNi_{0.5}Mn_{0.5}O_2$ cathode. The study demonstrates the superiority and suitability of $LiNi_{0.4}Mn_{0.4}Co_{0.2}O_2$ cathode over $LiNi_{0.5}Mn_{0.5}O_2$ and $LiNi_{0.45}Mn_{0.45}Co_{0.1}O_2$ cathodes at 1 C rate and up to 4.6 V limit.

Keywords Sol–gel method · Surfactant · Layered oxide cathodes · Lithium batteries · Spherical morphology

Introduction

Majority of the commercialized cathode materials for lithium ion batteries are based on $LiCoO_2$, but cobalt has environment-related problems that leave the door open to exploit alternative cathode materials [1]. Over the past several years, there have been concerted efforts to design Mn- or Ni-based layered $LiMO_2$ compounds with a view to find a less expensive and safer cathode material than $LiCoO_2$. However, $LiMnO_2$ and $LiNiO_2$ of $LiMO_2$ family have hampering issues like difficulty in the synthesis of stoichiometric and stable compounds and thus remain unsuitable for practical applications.

In an electronic stabilization approach, when Mn is partially substituted by Ni in equal concentration such as 1:1 in $LiMn_{0.5}Ni_{0.5}O_2$ compound, Ni is found to be in +2 state and Mn in +4 state, thus eliminating the adverse effects of Jahn–Teller distortion prone Mn^{3+} ions and becomes a successful cathode [2–4]. Basically, $LiNi_{0.5}Mn_{0.5}O_2$ cathode offers all the advantages of $LiCoO_2$ and a higher discharge capacity of 250 mA hg^{-1} (when charged up to 4.8 V) along with an apparently better chemical stability resulting from the electrochemical redox process of Ni^{2+}/Ni^{4+} via Ni^{3+} [2–6]. It also reduces the nickel content of $LiNiO_2$ electrode by 50 % without compromising its theoretical capacity (274 mA hg^{-1}).

However, the major drawback of $LiMn_{0.5}Ni_{0.5}O_2$ compound is that ~0.1Li^+ per formula unit is found in the transition metal layer of the O3-layered structure, which displaces an equivalent amount of Ni^{2+} to Li^+ layer [7, 8]. Such a disorder or mixing of Li^+ and Ni^{2+} in alternative layers may also result from the fact that they have similar ionic radii (Li^+=0.76 Å and Ni^{2+}=0.69 Å). On the other hand, presence of cobalt plays a critical role in minimizing the transition metal content in the lithium layer and enhances the electronic conductivity [9, 10]. Hence, lithium–nickel–manganese compounds with smaller amount of cobalt would be a better choice to prepare tailored cathode materials with better physical and electrochemical properties. Since the charge compensation in $LiNi_{0.5}Mn_{0.5}O_2$ proceeds via Ni^{2+} and Mn^{4+} in the transition metal layers, replacement of Ni^{2+} with an equal amount of M^{3+} (Co^{3+}) and Mn^{4+} will maintain the charge neutrality. Based on this simple concept, two solid solutions, viz., $LiNi_{0.45}Mn_{0.45}Co_{0.1}O_2$ and $LiNi_{0.4}Mn_{0.4}Co_{0.2}O_2$, were chosen for the present study along with the parent $LiNi_{0.5}Mn_{0.5}O_2$ cathode.

D. Bhuvaneswari · Gangulibabu · N. Kalaiselvi (✉)
CSIR—Central Electrochemical Research Institute,
Karaikudi 630 006, India
e-mail: kalaiselvicecri@gamil.com

It is well known that the electrochemical performance of any electrode material is highly sensitive to the synthesis procedure, which strongly affects the cationic distribution in lithium-transition metal oxides [11–13]. Towards this direction, literature is replete with results of this research group [14, 15] and other groups [16–19] on the citric acid-assisted sol–gel method, where the citric acid acts as a chelating agent to produce a transparent gel and to form the desired cathode materials. Quite different from such an approach, cetyltrimethyl ammonium bromide (CTAB), a known quaternary ammonium salt, has been exploited in the present study along with the chelating citric acid in order to obtain interconnected spherical morphology.

Initially, CTAB gets absorbed on the surface of precursor particles with its hydrophobic head inside and hydrophilic tail oriented away from the surface and thereby minimizes the friction between individual metal particles. Further, formation of metastable chelating complex in the form of a transparent gel is aided by the addition of citric acid and by adjusting the pH with NH_4OH. Herein, the selective capping effect of CTAB by its hydrophobic regions nucleating the surface plays a vital role in forming spherical particles without agglomeration via strong surface interaction and controls the growth of the same even upon high-temperature calcinations. The chelating citric acid forms a transparent gel at an alkaline pH (consisting of CTAB-facilitated spherical particles) and renders interconnectivity between the nano spherical particles to result in the formation of spherically interconnected surface morphology with a porous structure (Scheme 1). Such a formation of desired morphology with porosity will facilitate easy penetration of electrolyte and facile lithium ion transport, which is the significance of the study.

To sum up, the present study deals with the exploration of CTAB-coassisted sol–gel method in synthesizing phase pure and tailored cathodes of $LiNi_yMn_yCo_{1-2y}O_2$ [y=0.5, 0.45, and 0.4] family, wherein synergistic effect of synthesis method and the select concentration of Co^{3+} ions in improving the electrochemical performance has been investigated. Particularly, cycleability at extended voltage limits (4.5–4.8 V) and at different rates (0.1–1 C) has been studied.

Materials and methods

Synthesis procedure

The $LiNi_yMn_yCo_{1-2y}O_2$ [y=0.5, 0.45, and 0.4] active materials planned for the study were synthesized by adopting surfactant (CTAB) coassisted sol–gel method. Stoichiometric ratios of high purity starting materials, viz., $LiCOOCH_3$, $(CH_3COO)_2Co$, $(CH_3COO)_2Mn$, and $(CH_3COO)_2Ni$ (Alfa Aesar), were dissolved in water with stirring to get a homogeneous solution. To the solution, 0.01 M of CTAB surfactant was added dropwise and the stirring was continued for 1 h. Followed by this, an optimized amount of 1 M of citric acid as chelating agent was added. Further, ammonia solution was added drop wise to adjust the pH value of the solution between 8.5 and 9 and the process of stirring and heating (80 °C) was continued to get a transparent gel. The gel thus obtained was aged for 24 h in an oven and furnace-heated to 350 °C for about 12 h followed by calcination at 900 °C for about 5 h in air using alumina crucibles. Ultrafine $LiNi_yMn_yCo_{1-2y}O_2$ [y=0.5, 0.45, and 0.4] powders obtained after 900 °C were ground and subjected to characterization studies.

Details pertaining to electrode fabrication and the subsequent 2032 coin cell assembly are reported elsewhere [20]. Electrochemical characterizations were carried out on freshly fabricated 2032 coin cells consisting of lithium anode, synthesized $LiNi_yMn_yCo_{1-2y}O_2$ [y=0.5, 0.45, and 0.4] cathodes individually, and a nonaqueous electrolyte consisting of 1 M $LiPF_6$ dissolved in 1:1 v/v EC/PC with a Celgard separator.

Physical and electrochemical characterizations

Phase characterization was done by powder X-ray diffraction technique on a PANalytical X'pert PRO X-ray diffractometer using Ni-filtered Cu Kα radiation (=1.5406 Å) in the 2θ range 15–70° at a scan rate of 0.04° s^{-1}. The lattice parameters were determined using the HighScore Plus software package. Surface chemical compositions of individual cathode materials were measured using X-ray photoelectron spectroscopy on a Physical Electronics model 5400 X-ray photoelectron spectrometer using an Mg Kα excitation source. The surface morphology and particle size of synthesized samples were examined by scanning electron microscopy (SEM, HITACHI S–3000 H, and Japan) and transmission electron microscopy (TEM, FEI-Tecnai-20 G2). Electrochemical cycling behavior (CV) was performed using an AutoLab electrochemical workstation and the charge–discharge studies were carried out on ARBIN charge–discharge cycle life tester.

Result and discussion

Powder diffraction studies—structural characterization

Powder diffraction pattern recorded for $LiNi_yMn_yCo_{1-2y}O_2$ [y=0.5, 0.45, and 0.4] compounds are depicted in Fig. 1a–c. All the diffraction peaks could be indexed to α-$NaFeO_2$-type of structure (space group R-3m) that forms an fcc lattice with a distortion in the c direction, as indicated by the clear splitting of the (006)/(102) and (108)/(110) peaks.

Scheme 1 Formation of interconnected spherical particles facilitated by CTAB-coassisted sol–gel method

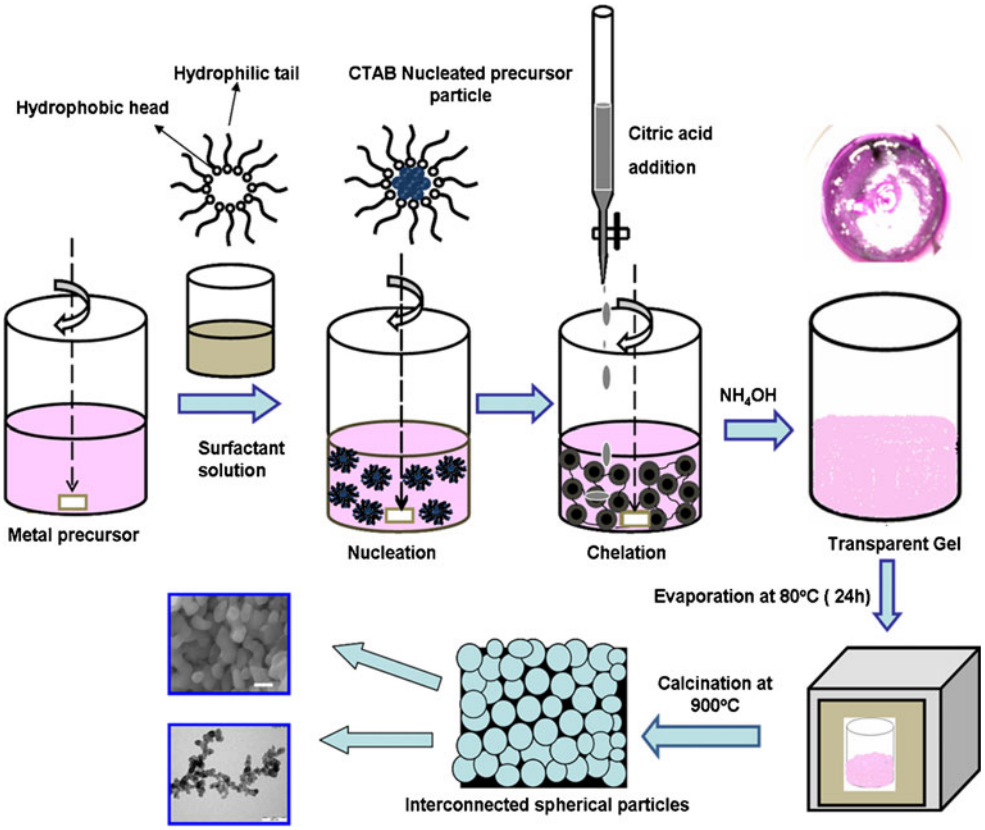

It is well known that a good resolution of (006)/(102) and (108)/(110) diffraction pairs is typical of an ideal layered structure with superior crystallinity, good hexagonal ordering, and better intercalation characteristics [21, 22]. Figure 1 evidences the presence of distinct splitting of (006) and (102) doublets at $2\theta = 38.5°$ and those of (108) and (110) at $2\theta = 65°$ for $LiNi_yMn_yCo_{1-2y}O_2$ [y=0.45 and 0.4] compounds, which is in favor of the formation of good layered structure. It is further understood from the cell parameters and the degree of cation ordering derived from XRD (Table 1), i.e., the increasing $c/3a$ ratio from 1.637 to 1.652 with the increase in cobalt content substantiated the presence of perfectly formed layered lattice [23, 24]. Similarly, the $I_{(003)}/I_{(104)}$ ratio increases from 1.15 to 1.38 which is greater than unity with an increase in the concentration of cobalt and the same is an indication of lowering the degree of cation mixing [25, 26]. Hence the role of Co^{3+} in minimizing the cation mixing of pristine $LiNi_{0.5}Mn_{0.5}O_2$ lattice could be understood. The R value refers to the ratio of the sum of diffraction intensity of (006) and (102) to the diffraction intensity of (101) which measures the cation disorder. This

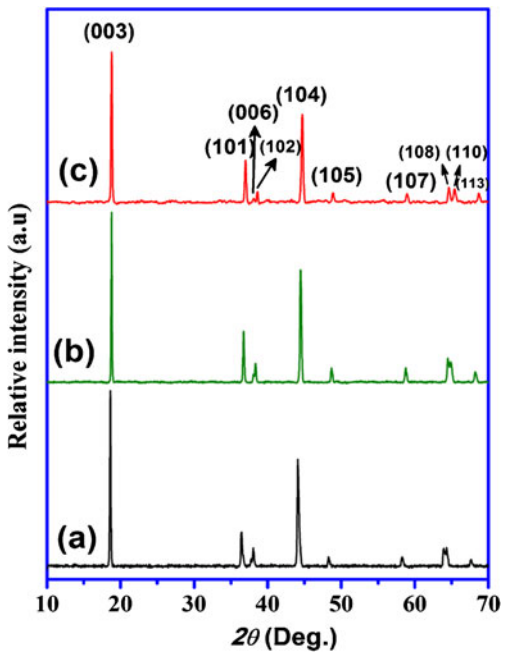

Fig. 1 X-ray diffraction pattern of **a** $LiNi_{0.5}Mn_{0.5}O_2$; **b** $LiNi_{0.45}Mn_{0.45}Co_{0.1}O_2$; and **c** $LiNi_{0.4}Mn_{0.4}Co_{0.2}O_2$ synthesized by CTAB-coassisted sol–gel method

Table 1 Physical parameters calculated for $LiNi_yMn_yCo_{1-2y}O_2$ [y=0.5, 0.45, and 0.4] compounds

Physical parameters	a (Å)	c (Å)	c/3a	$I_{(003)}/I_{(104)}$	R factor $[(I_{(006)}+I_{(102)})/I_{(101)}]$
$LiNi_{0.5}Mn_{0.5}O_2$	2.894	14.217	1.637	1.15	0.52
$LiNi_{0.45}Mn_{0.45}Co_{0.1}O_2$	2.869	14.174	1.647	1.35	0.45
$LiNi_{0.4}Mn_{0.4}Co_{0.2}O_2$	2.861	14.182	1.652	1.38	0.40

is found to be the lowest for $LiNi_yMn_yCo_{1-2y}O_2$ [y=0.45 and 0.4] compounds and suggests that the hexagonal ordering is better.

Electron microscopy studies—particle size

Presence of 200 nm secondary particles of $LiNi_yMn_yCo_{1-2y}O_2$ [y=0.5, 0.45, and 0.4] compounds prepared by surfactant-coassisted sol–gel method are evidenced by transmission electron microscopy (Fig. 2). Particularly, homogeneous distribution of spherical particles with interconnected crystals is seen from the TEM images (Fig. 2a–c). Figure 2d shows the representative SEM image of $LiNi_yMn_yCo_{1-2y}O_2$ [y=0.5, 0.45, and 0.4] compounds, wherein spherical particles with interconnected morphology is found to get maintained even after furnace calcination at 900 °C. Unlike citric acid-assisted sol–gel method (inset of Fig. 2d), wherein presence of crystalline particles is seen without any desired spherical or interconnected morphology, the currently adopted CTAB-coassisted sol–gel method has produced interconnected spherical particles and the same could be attributed to the selective capping (or) nucleation effect of CTAB as a surfactant. Further, $LiNi_yMn_yCo_{1-2y}O_2$ [y=0.5, 0.45, and 0.4] compounds synthesized with CTAB surfactant shows uniformly distributed and size reduced (200 nm) primary particles that are properly interconnected to form a porous network, which in turn would facilate better penetration of electrolyte and improve the electrochemical performance. Hence, it is learnt from the current study that the newly adopted surfactant-coassisted sol–gel method is advantageous over the conventional solid state [27], mixed hydroxide [28], and solution-assisted combustion [29] methods in synthesizing layered $LiNi_yMn_yCo_{1-2y}O_2$ [y=0.5, 0.45, and 0.4] compounds with desired morphology.

X-ray photoelectron spectroscopy-elemental composition of cathode material

X-ray photoelectron spectroscopy (XPS) was employed to confirm the oxidation state of metal ions present in $LiNi_yMn_yCo_{1-2y}O_2$ [y=0.5, 0.45, and 0.4] compounds. From Fig. 3, it is evident that the binding energy (BE) values of Ni $2p_{3/2}$, Co $2p_{3/2}$, and Mn $2p_{3/2}$ of $LiNi_yMn_yCo_{1-2y}O_2$ [y=0.5, 0.45, and 0.4] compounds are in good agreement with the reported values [30, 31]. The curve fitting of $LiNi_{0.5}Mn_{0.5}O_2$ Ni $2p_{3/2}$ signal at 855 eV indicates [30, 31] a slight shift in energy towards higher side compared to those of $LiNi_{0.45}Mn_{0.45}Co_{0.1}O_2$ and $LiNi_{0.4}Mn_{0.4}Co_{0.2}O_2$ compounds, which may be correlated to the effect of cationic mixing. However, the presence of an additional and a characteristic satellite peak noted with the Ni $2p_{3/2}$ signal, corresponding to the multi-electron excitation behavior, confirms the oxidation state of Ni as +2 in all the $LiNi_yMn_yCo_{1-2y}O_2$ compounds. The best fit for the Co $2p_{3/2}$ spectrum gives a BE value, which is matching with the value reported by Shaju et al. [32] for Co^{3+} ions. Similarly, the Mn XPS spectra that has a major peak located at a binding energy value of 642.2 eV for $LiNi_{0.45}Mn_{0.45}Co_{0.1}O_2$ and $LiNi_{0.4}Mn_{0.4}Co_{0.2}O_2$ compounds matches with the BE reported for Mn^{4+} ions [33]. Here again, a small shift towards higher energy side is observed for $LiNi_{0.5}Mn_{0.5}O_2$ compounds, which may also be correlated to the possible presence of cation mixing. Based on these results, the individual oxidation state of Ni, Mn, and Co atoms in the currently

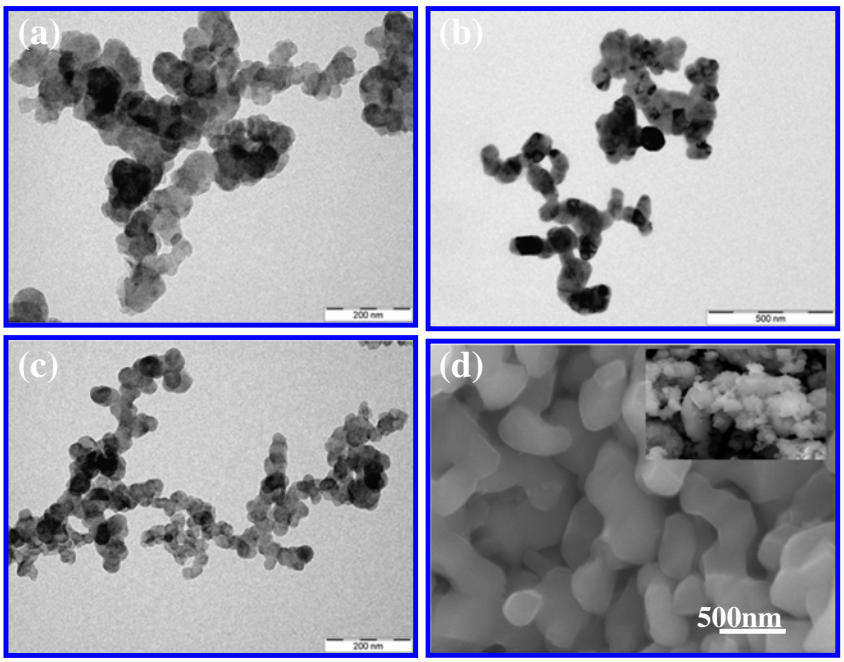

Fig. 2 TEM images of CTAB-coassisted sol–gel synthesized: **a** $LiNi_{0.5}Mn_{0.5}O_2$; **b** $LiNi_{0.45}Mn_{0.45}Co_{0.1}O_2$; **c** $LiNi_{0.4}Mn_{0.4}Co_{0.2}O_2$; and **d** typical SEM image of $LiNi_yMn_yCo_{1-2y}O_2$. *Inset* typical SEM image of citric acid-assisted sol–gel synthesized $LiNi_{0.4}Mn_{0.4}Co_{0.2}O_2$

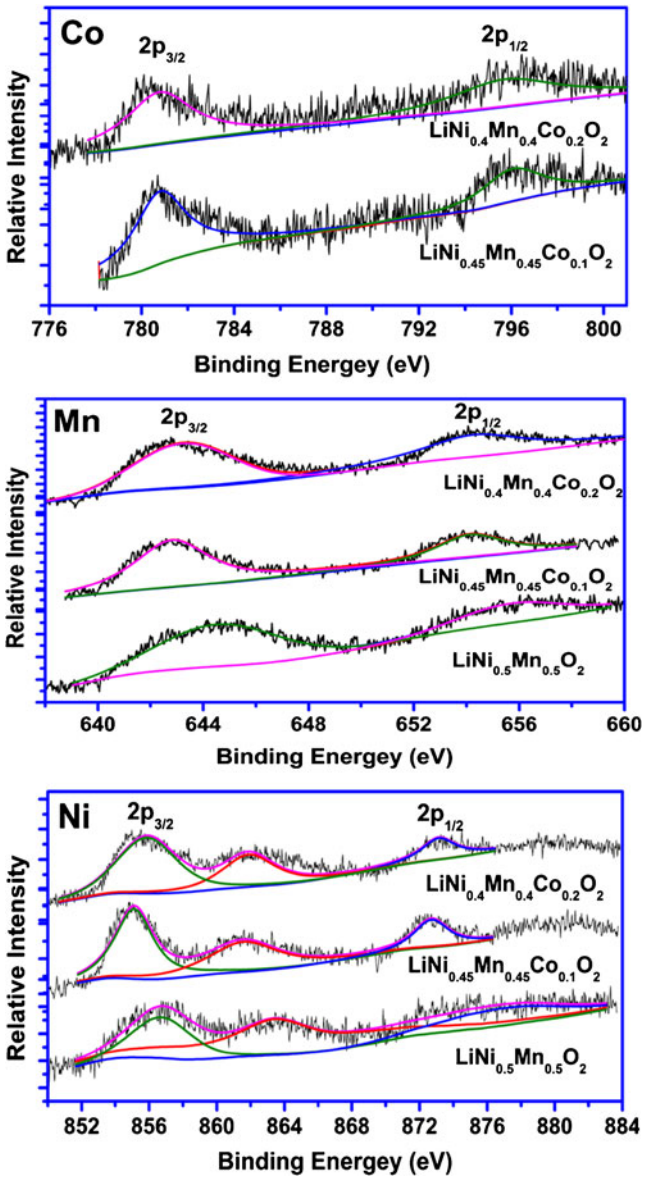

Fig. 3 X-ray photoelectron spectroscopy recorded for $LiNi_yMn_yCo_{1-2y}O_2$ compound

synthesized $LiNi_yMn_yCo_{1-2y}O_2$ [y=0.5, 0.45, and 0.4] compounds has been confirmed as +2, +4, and +3, respectively, and the charge neutrality of synthesized compounds is thus understood.

Electrochemical characterizations

The electrochemical behavior of synthesized cathodes was evaluated using 2032 coin cells containing lithium foil as anode and the synthesized compounds as cathode individually, wherein the investigation was carried out initially at C/10 rate in the potential range between 2.5 and 4.6 V. Figure 4 shows the charge and discharge profile of $LiNi_yMn_yCo_{1-2y}O_2$ [y=0.5, 0.45, and 0.4] cathodes, wherein the first discharge

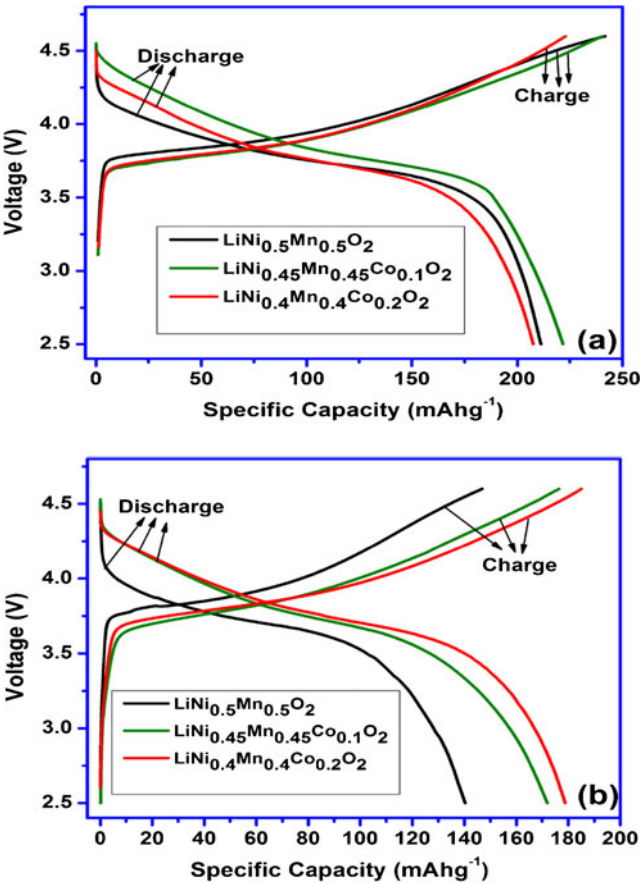

Fig. 4 Voltage vs. capacity behavior of $LiNi_yMn_yCo_{1-2y}O_2$ (y=0.5, 0.45, and 0.4) cathode materials in the potential range of 2.5~4.6 V corresponding to **a** first cycle and **b** 50th cycle

capacity of $LiNi_{0.5}Mn_{0.5}O_2$, $LiNi_{0.45}Mn_{0.45}Co_{0.1}O_2$, and $LiNi_{0.4}Mn_{0.4}Co_{0.2}O_2$ is found to be 210, 222, and 206 mA hg^{-1}, respectively. Subsequently, an initial irreversible capacity loss of 30, 22, and 16 mA hg^{-1} has been exhibited by $LiNi_{0.5}Mn_{0.5}O_2$, $LiNi_{0.45}Mn_{0.45}Co_{0.1}O_2$, and $LiNi_{0.4}Mn_{0.4}Co_{0.2}O_2$ cathodes, which is not unusual. Further, such a reduced irreversible capacity loss of 16 mA hg^{-1} exhibited by the currently synthesized $LiNi_{0.4}Mn_{0.4}Co_{0.2}O_2$ cathode indicates the superiority of the same, based on the reported behavior [10, 26] in the literature. On the other hand, progressive discharge capacity values of 140, 172, 179 mA hg^{-1} have been observed for $LiNi_{0.5}Mn_{0.5}O_2$, $LiNi_{0.45}Mn_{0.45}Co_{0.1}O_2$, and $LiNi_{0.4}Mn_{0.4}Co_{0.2}O_2$ cathodes at the end of the 50th cycle (Fig. 4), thus suggesting that 20 % cobalt addition is beneficial in minimizing the capacity fade of native $LiNi_{0.5}Mn_{0.5}O_2$ cathode, via hexagonal ordering of lithium and nickel ions. Further, maintenance of discharge plateau at 3.8 V and the absence of plateau around 4.0 V exhibited up to 50 cycles confirm the absence of possible structural changes of layered $LiNi_yMn_yCo_{1-2y}O_2$ [y=0.5, 0.45, and 0.4] cathodes into spinel-related phases [34]. Such an improved structural stabilization is attributed to the presence of Mn^{4+} that maintains

the oxide network favorable for facile lithium intercalation/de-intercalation upon extended cycling.

The cycling behavior of $LiNi_yMn_yCo_{1-2y}O_2$ [y=0.5, 0.45, and 0.4] cathodes at 0.1 and 0.2 C rate is furnished in Fig. 5. As mentioned already, an initial discharge capacity of 210, 222, and 206 mA hg^{-1} has been exhibited by $LiNi_{0.5}Mn_{0.5}O_2$, $LiNi_{0.45}Mn_{0.45}Co_{0.1}O_2$, and $LiNi_{0.4}Mn_{0.4}Co_{0.2}O_2$ cathodes at 0.1 C rate with reduced second cycle discharge capacity values such as 176, 213, and 192 mA hg^{-1}, respectively. Interestingly, $LiNi_{0.4}Mn_{0.4}Co_{0.2}O_2$ cathode with 192 mA hg^{-1} of second cycle discharge capacity exhibited better capacity retention (93 %) and lesser capacity fade (7 %) up to 50 cycles. In other words, the overall capacity retention of $LiNi_yMn_yCo_{1-2y}O_2$ [y=0.5, 0.45, and 0.4] cathodes calculated for 50 cycles (with respect to second cycle discharge capacity value) is found to be 78, 82, and 93 %, respectively. Similarly, when charge–discharge cycling was performed at 0.2 C rate, $LiNi_{0.4}Mn_{0.4}Co_{0.2}O_2$ cathode exhibited a capacity as high as 160 mA hg^{-1} along with a capacity retention of 98 %, compared to those of $LiNi_{0.5}Mn_{0.5}O_2$ (142 mA hg^{-1}) and $LiNi_{0.45}Mn_{0.45}Co_{0.1}O_2$ (150 mA hg^{-1}) with a capacity retention of 89 and 95 %, respectively. Such an improved electrochemical behavior of $LiNi_{0.4}Mn_{0.4}Co_{0.2}O_2$ cathode has been endorsed to the synergistic effect of spherically formed interconnected particles obtained from CTAB-coassisted sol–gel method and the optimum cobalt substitution (20 %) that minimizes the cation disorder.

Further, with a view to investigate the rate capability behavior of $LiNi_yMn_yCo_{1-2y}O_2$ [y=0.5, 0.45, and 0.4] cathodes, electrodes of synthesized compounds were subjected to charge–discharge cycling with different C rates and the observed capacity values are depicted in Fig. 6. The discharge capacity of $LiNi_{0.5}Mn_{0.5}O_2$ is 210 mA hg^{-1} at a 0.1-C rate and the same gets decreased to 70 mA hg^{-1} at 1 C rate. Interestingly, 10 % of cobalt-doped $LiNi_{0.45}Mn_{0.45}Co_{0.1}O_2$ cathode exhibits the highest discharge capacity of 222 mA hg^{-1} (compared to the rest of the cathodes at 0.1 C rate) but suffers from significant capacity fade, as evident from the reduced capacity value of 94 mA hg^{-1} exhibited observed at 1 C rate. On the other hand, $LiNi_{0.4}Mn_{0.4}Co_{0.2}O_2$ cathode exhibits a nominal discharge capacity of 206 mA hg^{-1} at 0.1 C rate and an appreciable capacity value of 163, 131, and 109 mA hg^{-1} at higher discharge rates such as 0.2, 0.5, and 1 C rate, respectively. As mentioned earlier, such an improved rate capability behavior of $LiNi_{0.4}Mn_{0.4}Co_{0.2}O_2$ cathode is also attributed to the optimum addition of cobalt (20 %) that minimizes the cation disorder in the pristine $LiNi_{0.5}Mn_{0.5}O_2$ lattice and the formation of interconnected spherical grains obtained from CTAB-coassisted sol–gel method.

Based on the encouraging results obtained for $LiNi_{0.4}Mn_{0.4}Co_{0.2}O_2$ cathode, an explorative attempt to investigate the CV behavior of the same at different voltages such as 4.4, 4.5, 4.6, 4.7, 4.8, and 4.85 V has been made with the scan rate of 0.1 mV s^{-1} (Fig. 7), mainly to understand the

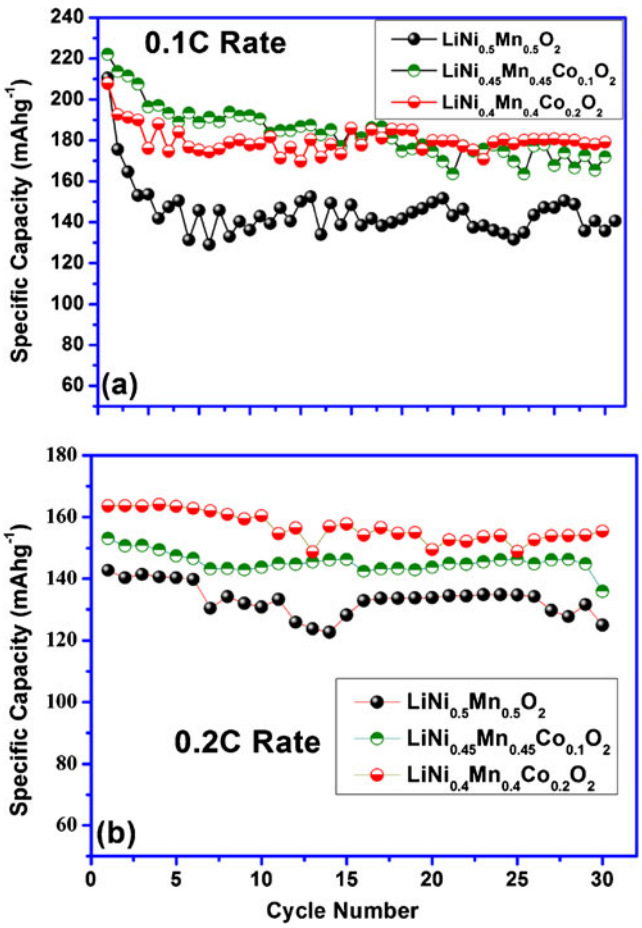

Fig. 5 Cycling performance of $LiNi_yMn_yCo_{1-2y}O_2$ (y=0.5, 0.45, and 0.4) cathode under the influence of 0.1 and 0.2 C rate

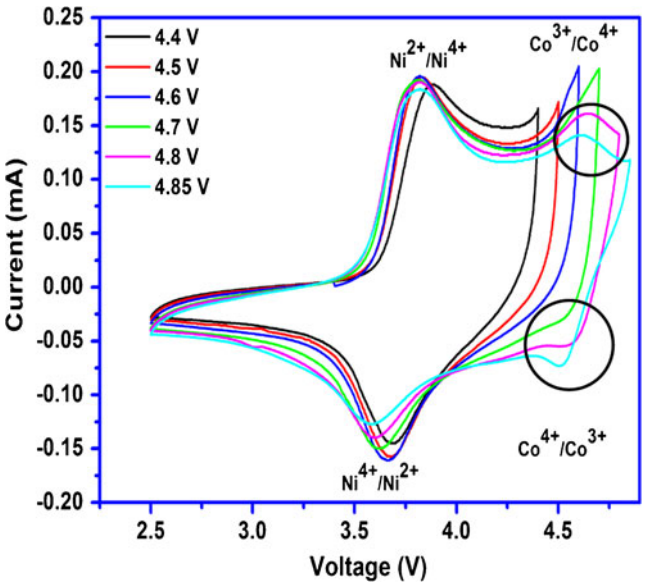

Fig. 6 Rate capability behavior of $LiNi_yMn_yCo_{1-2y}O_2$ (y=0.5, 0.45, and 0.4) cathodes at different C rates

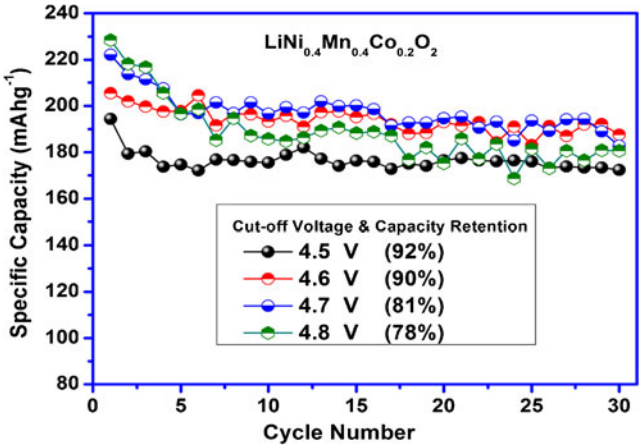

Fig. 7 Cyclic voltammograms of $LiNi_{0.4}Mn_{0.4}Co_{0.2}O_2$ cathode at different cutoff voltages

effect and extent of individual transition metals in imparting the specific capacity. The CV recorded with 4.4 V cutoff voltage limit consists of a redox couple at 3.81 and 3.68 V corresponding to Ni^{2+}/Ni^{4+} pair, and Mn^{4+}, being an electrochemically inactive species, gives rise to no CV signal throughout the study, which is justifiable. Alternatively, CV recorded up to 4.6 V and at higher cutoff voltage limits (4.7 to 4.85 V) consists of another redox pair at 4.58 and 4.51 V, corresponding to the presence of Co^{3+}/Co^{4+} redox pair. Hence, apart from an understanding on the facile intercalation and de-intercalation behavior of Li^+ ions in $LiNi_{0.4}Mn_{0.4}Co_{0.2}O_2$ cathode and the respective oxidation states of Ni^{+2}, Co^{+3}, and Mn^{+4} ions, significant role of Co^{+3} ions in improving the electrochemical behavior of the same has also been substantiated from CV studies.

The charge–discharge behavior of $LiNi_{0.4}Mn_{0.4}Co_{0.2}O_2$ cathode synthesized using surfactant-coassisted sol–gel method at different cutoff voltages (0.1 C rate) has been furnished in Fig. 8 and the observed capacity fade values are given in Table 2. An increasing capacity value from 194 to

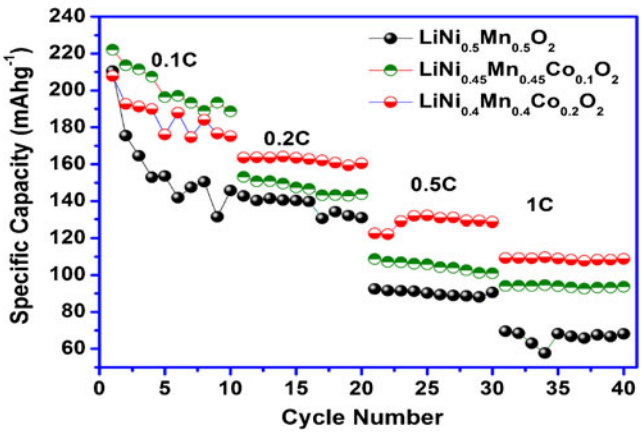

Fig. 8 Cycling performance of $LiNi_{0.4}Mn_{0.4}Co_{0.2}O_2$ cathode at different cutoff voltages (2.5~4.5, 4.6, 4.7, and 4.8 V)

Table 2 The initial and 30th cycle discharge capacity values and corresponding capacity fade of $LiMn_{0.4}Ni_{0.4}Co_{0.2}O_2$ cathode at different cutoff voltages

Voltage range	Discharge Capacity (mA hg^{-1})		Capacity fade (%)
	Initial	30th cycle	
2.5~4.5 V	180	172	5
2.5~4.6 V	206	187	7
2.5~4.7 V	214	182	15
2.5~4.8 V	218	181	17

228 mA hg^{-1} has been observed with an increase in the upper cutoff voltage from 4.5 to 4.8 V. Simultaneously, an increasing capacity fade of about 15 and 17 % has been observed up to 30 cycles, when the cell was charged to 4.7 and 4.8 V limits, respectively. This could be correlated to the slight shift in redox peaks observed in CV exhibited by $LiNi_{0.4}Mn_{0.4}Co_{0.2}O_2$ cathode, especially when cycled beyond 4.6 V. Interestingly, $LiNi_{0.4}Mn_{0.4}Co_{0.2}O_2$ cathode exhibited reduced capacity fade behavior (7 %) and an enhanced capacity value (192 mA hg^{-1}), especially when cycled up to 4.6 V compared to those of 4.7 and 4.8 V limits. On the other hand, cycling up to 4.5 V renders much reduced capacity fade behavior (5 %) but at the expense of highly reduced initial and progressive capacity values (180 mA hg^{-1}). Therefore, it is evident from the present study that $LiNi_{0.4}Mn_{0.4}Co_{0.2}O_2$ cathode synthesized by CTAB-coassisted sol–gel method exhibits lesser capacity fade (7 %) and higher capacity value (192 mA hg^{-1}) at 4.6 V limit, compared to those reported at reduced potential windows such as 4.3 and 4.5 V [11, 26]. Such an improved electrochemical behavior of $LiNi_{0.4}Mn_{0.4}Co_{0.2}O_2$ cathode has been endorsed to the synergistic effect of interconnected and spherically shaped particles (~200 nm) derived from surfactant-coassisted sol–gel method and the perfect layeredness obtained by using an optimum (20 %) amount of cobalt in the solid solution.

Conclusions

$LiNi_{0.5}Mn_{0.5}O_2$, $LiNi_{0.45}Mn_{0.45}Co_{0.1}O_2$, and $LiNi_{0.4}Mn_{0.4}Co_{0.2}O_2$ compounds were prepared at 900 °C using CTAB-coassisted sol–gel method. The Co^{+3} introduction in $LiNi_{0.5}Mn_{0.5}O_2$ compound helps in increasing the reversible capacity and rate capability. Among the $LiNi_yMn_yCo_{1-2y}O_2$ [y=0.5, 0.45, and 0.4] compounds, $LiNi_{0.4}Mn_{0.4}Co_{0.2}O_2$ cathode exhibited superior discharge capacity (192 mA hg^{-1}) and with an excellent capacity retention (93 %) for 50 cycles, and its rate capability at 1 C rate and cycling behavior up to 4.6 V are found to be satisfactory compared to those of $LiNi_{0.5}Mn_{0.5}O_2$ and

$LiNi_{0.45}Mn_{0.45}Co_{0.1}O_2$ cathodes. The study recommends that the currently adopted surfactant-coassisted sol–gel method is yet another potential approach to synthesize $LiNi_yMn_yCo_{1-2y}O_2$ [y=0.5, 0.45, and 0.4] compounds with interconnected spherical grains which are responsible for the improved electrochemical properties. Further, the suitability of $LiNi_{0.4}Mn_{0.4}Co_{0.2}O_2$ cathode for high-rate (1 C) lithium battery applications is believed to result from the synergistic effect of synthesis method and the selection of optimum amount of (20 %) Co^{3+} concentration that renders required cation ordering.

Acknowledgments Among the authors, D. Bhuvaneswari and Gangulibabu are thankful to the Council of Scientific and Industrial Research, India for financial support through senior research fellowship.

References

1. Ni JF, Zhou HH, Chen JT, Zhang XX (2005) Mater Lett 59:2361–2365
2. Yabuuchi N, Ohzuku TJ (2003) Power Sources 119–121:171–174
3. Ohzuku T, Makimura Y (2001) Chem Lett 30:642–643
4. Xiao J, Chernova NA, Whittingham MS (2010) Chem Mater 22:1180
5. Ellis BL, Lee KT, Nazar LF (2010) Chem Mater 22:691–714
6. Liu Y, Chen B, Cao F, Zhao X, Yuan J (2011) J Mater Chem 21:10437–10441
7. Kobayashi H, Arachi Y, Kageyama H, Tatsumi K (2004) J Mater Chem 14:40–42
8. Sakamoto K, Hirayama M, Konishi H, Sonoyama N, Dupre N, Guyomard D, Tamura K, Mizuki J, Kanno R (2010) Phys Chem Chem Phys 12:3815–3823
9. Whittingham MS (2004) Chem Rev 104:4271–4301
10. Xiao J, Chernova NA, Whittingham MS (2008) Chem Mater 20:7454–7464
11. Bruce PG, Scrosati B, Tarascon JM (2008) Angew Chem Int Ed 47:2930–2946
12. Ahn D, Koo YM, Kim MG, Shin N, Park J, Eom J, Cho J, Shin TJ (2010) J Phys Chem C 114:3655–3680
13. He P, Wang HR, Qi L, Osaka TJ (2006) Power Sources 160:627–632
14. Jayaprakash N, Sathiyanarayanan K, Kalaiselvi N (2007) Electrochim Acta 52:2453–2460
15. Jayaprakash N, Kalaiselvi N, Doh CH, Gangulibabu, Bhuvaneswari D (2010) J Appl Electrochem 40:2193–2202
16. Huang ZD, Liu XM, Oh SW, Zhang B, Ma BC, Kim JK (2011) J Mater Chem 21:10777–10784
17. Song WS, Choi HN, Kim YS, Yang H (2010) J Mater Chem 20:6929–6934
18. Sun YK, Oh IH, Kimc KY (1997) J Mater Chem 7:1481–1485
19. Brinker CJ, Scherer GW (1990) Sol-gel science: the physics and chemistry of sol-gel processing. Academic Press Inc., San Diego, CA
20. Gangulibabu, Bhuvaneswari D, Kalaiselvi N, Jayaprakash N, Periasamy P (2009) J Sol Gel Sci Techno 49:137–144
21. Zhang L, Wang X, Muta T, Li D, Noguchi H, Yoshio M, Ma R, Takada K, Sasaki T (2006) J Power Sources 162:629–625
22. Wang J, Yao X, Zhou X, Liu Z (2011) J Mater Chem 21:2544–2549
23. Carley AF, Jackson SD, O'Shea JN, Roberts MW (1999) Surf Sci 440:L868–L864
24. Ngala JK, Chernova NA, Ma M, Mamak M, Zavalij PY, Whittingham MS (2004) J Mater Chem 14:214–220
25. Reale P, Privitera D, Panero S, Scrosati B (2007) Solid State Ionics 178:1390–1397
26. Liu H, Wu YP, Rahm E, Holze R, Wu HQ (2004) J Solid State Chem 8:450–466
27. Wu Q, Li X, Yan M, Jiang Z (2003) Electrochem Commun 5:878–882
28. Lu Z, MacNeil DD, Dahn JR (2001) Electrochem Solid State Lett 4:A191–A194
29. Patoux S, Doeff MM (2004) Electrochem Commun 6:767–772
30. Casella G, Guascito MR, Sannazzaro MG (1999) J Electroanal Chem 462:202–210
31. Zhao Y, Fan YEL, Qiu Y, Yang S (2007) Electrochim Acta 52:5873–5878
32. Shaju KM, Subba Rao GV, Chowdari BVR (2002) Solid State Ionics 69:152–153
33. Shaju KM, Subba Rao GV, Chowdari BVR (2002) Electrochim Acta 48:145–151
34. Hwang BJ, Tsai YW, Chen CH, Santhanam R (2003) J Mater Chem 13:1962–1968